THE JOURNAL OF BIOLOGICAL CHEMISTRY
Vol. 270, No. 51, Issue of December 22, pp. 30532–30544, 1995

Printed in U.S.A.

Spectroscopic and Kinetic Properties of Unphosphorylated Rat Hepatic Phenylalanine Hydroxylase Expressed in *Escherichia coli*

COMPARISON OF RESTING AND ACTIVATED STATES*

(Received for publication, June 26, 1995, and in revised form, August 30, 1995)

T. Joseph Kappock‡§, Paul C. Harkins¶, Steven Friedenberg‡, and John P. Caradonna‡‖

From the ‡Department of Chemistry, Yale University, New Haven, Connecticut 06520-8107 and the ¶Bass Center for Molecular Biophysics and Biochemistry, Yale University, New Haven, Connecticut 06520-8114

The non-heme iron-dependent metalloenzyme, rat hepatic phenylalanine hydroxylase (EC 1.14.16.1; phenylalanine 4-monooxygenase (PAH)) was overexpressed in *Escherichia coli* and purified to homogeneity, allowing a detailed comparison of the kinetic, hydrodynamic, and spectroscopic properties of its allosteric states. The homotetrameric recombinant enzyme, which is highly active and contains 0.7–0.8 iron atoms per subunit, is identical to the native enzyme in several properties: K_m, 6-methyltetrahydropterin = 61 μM and L-Phe = 170 μM; V_{max} = 9 s^{-1} (compared to 45 μM, 180 μM, and 13 s^{-1} for the rat hepatic enzyme). L-Phe and lysolecithin treatment induce the $rPAH^T \rightarrow rPAH^R$ (where r is recombinant) allosteric transformation necessary for rPAH activity. Characteristic changes in the fluorescence spectra, increased hydrophobicity, a large activation energy barrier, and a 10% volume increase of the tetrameric structure are consistent with a significant reorganization of the protein following allosteric activation. However, optical and EPR spectroscopic data suggest that only minor changes occur in the primary coordination sphere (carboxylate/histidine/water) of the catalytic iron center. Detailed steady state kinetic investigations, using 6-methyltetrahydropterin as cofactor and lysolecithin as activator, indicate rPAH follows a sequential mechanism. A catalytic Arrhenius E_{act} of 14.6 ± 0.3 kcal/mol subunit was determined from temperature-dependent stopped-flow kinetics data. rPAH inactivates during L-Phe hydroxylation with a half-life of 4.3 min at 25 °C, corresponding to an Arrhenius E_{act} of 10 ± 1 kcal/mol subunit for the inactivation process. Catechol binding (2.4×10^6 M^{-1}) is shown to occur only at catalytically competent iron sites. Ferrous rPAH binds NO, giving rise to an S_T = ½ spin system.

Phenylketonuria (PKU)[1] is a relatively common inborn error of amino acid metabolism caused by the accumulation of neurotoxins derived from L-phenylalanine. A major clinical manifestation of untreated PKU is progressive postnatal brain damage leading to severe mental retardation that is thought to arise from the decreased protection of myelin proteins against proteolytic degradation. This degenerative process may be slowed in newborns only through the immediate and rigorous implementation of a controlled L-Phe diet. The Mendelian inheritance pattern of this degenerative condition indicates there is a single detoxifying enzyme absent in phenylketonurics. Phenylketonuric liver biopsies show severely reduced or absent phenylalanine hydroxylase (EC 1.14.16.1; L-phenylalanine tetrahydropterin:oxygen oxidoreductase (PAH)) activity, which ordinarily regulates blood [L-Phe] and prevents PKU. Worldwide screening efforts have allowed the identification of over 150 PAH mutations that cause PKU (1).

Mammalian PAH is a soluble, homotetrameric protein (molecular mass = 51.7 kDa) whose activity depends upon the presence of a single non-heme iron center per subunit (2). Rat hepatic PAH is the most extensively studied of the tetrahydrobiopterin (BH_4)-dependent amino acid hydroxylases (3, 4), a highly homologous family of enzymes that includes TyrH and TrpH. These brain enzymes perform the rate-limiting steps in the biosynthesis of catecholamine neurotransmitters and serotonin, respectively. All of the pterin-dependent hydroxylases are thought to contain similar active sites, due to the very high conservation of "catalytic domain" residues, as well as their similar substrates, common biopterin cofactor, and shared sensitivity to potentially chelating inhibitors (3, 5, 6). The highest level of DNA sequence homology among these enzymes, as well as the location of many of the more severe PKU mutations, occurs in PAH exon 7, which may be of particular importance because it is a constituent of the catalytic core.

PAH interacts in a dual fashion with each of its substrates; in addition to their roles in the catalytic cycle, L-Phe is the obligate allosteric activator of PAH, while reduction of resting state ferric PAH to the ferrous state is performed by BH_4 (7, 8). Formation of reduced, phenylalanine-activated PAH is concurrent with the appearance of a catalytically competent species (3).

Activation by L-Phe is typical of a catabolic enzyme's feed-forward response to substrate (Fig. 1). The slow conversion of low activity, T state PAH (PAH^T) to R state PAH (PAH^R-[L-Phe]) is facilitated by phosphorylation and inhibited by BH_4 (9–11). PAH is isolated from liver in a partially phosphorylated state, due to regulation by phosphorylation/dephosphorylation at Ser-16 (12). The amino acid substrate specificity is diminished following substrate activation or limited proteolysis (ex-

* This work was supported in part by the Donors of the Petroleum Research Fund administered by the American Chemical Society (25953AC) and the Camille and Henry Dreyfus and Alfred P. Sloan Foundations. The costs of publication of this article were defrayed in part by the payment of page charges. This article must therefore be hereby marked "*advertisement*" in accordance with 18 U.S.C. Section 1734 solely to indicate this fact.

§ Howard Hughes Medical Institute Predoctoral Fellow.

‖ To whom correspondence should be addressed: Dept. of Chemistry, Yale University, P.O. Box 208107, New Haven, CT 06520-8107. Tel.: 203-432-5221. Fax: 203-432-6144; E-mail: jpc@miles.chem.yale.edu.

[1] The abbreviations used are: PKU, phenylketonuria; PAH, phenylalanine hydroxylase; BH_4, tetrahydrobiopterin or (6*R*)-[L-*erythro*-dihydroxypropyl]-5,6,7,8-tetrahydropterin; 6-MPH_4, 6-methyl-5,6,7,8-tetrahydropterin; 6-MPH_2, 6-methyl-7,8-dihydropterin; *q*-6-MPH_2, *quinonoid*-6-methyl-7,8-dihydropterin; TyrH, tyrosine hydroxylase; TrpH, tryptophan hydroxylase; MOPS, 4-morpholinepropanesulfonic acid; DTT, dithiothreitol; PAGE, polyacrylamide gel electrophoresis; rPAH, recombinant PAH; LMCT, ligand-to-metal charge-transfer.

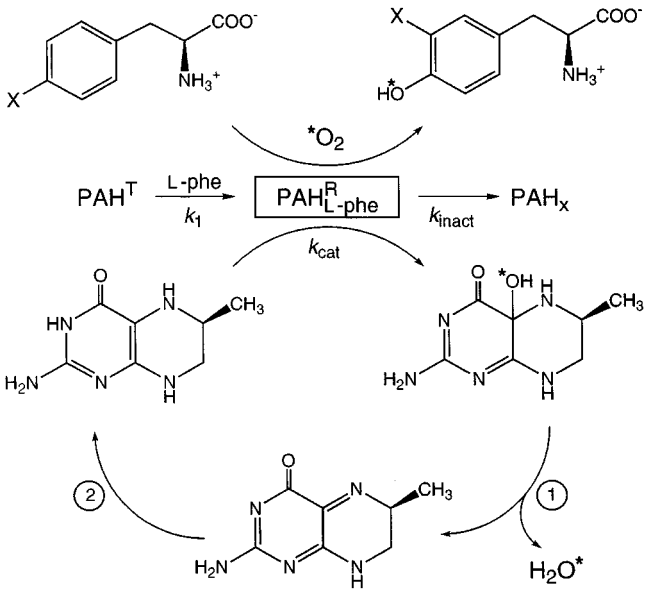

FIG. 1. **Catalytic scheme for PAH.** PAH^T = resting/T state PAH, PAH^R = activated/R state PAH, and PAH_x = inactivated PAH; k_1, k_{inact}, and k_{cat} are all apparent first-order rate constants for the allosteric activation, irreversible inactivation, and catalytic processes. The obligate prereduction of PAH has been omitted for clarity; only $\{Fe^{2+}\}$ PAH^R is catalytically active. The NIH shift of *para-X* to *meta-X* is known to occur when $X = {}^2H$, ${}^3H$, chlorine, bromine, or CH_3. Also shown is the recycling of the initial 4a-hydroxypterin product back to reduced tetrahydropterin. In *reaction 1*, a spontaneous dehydration reaction that is accelerated in liver by 4a-carbinolamine dehydratase/DCoH, *q*-6-MPH_2 is formed. In *reaction 2* this unstable oxidized form of the pterin is reduced, either by dihydropteridine reductase/NADPH (in liver and in the Nielsen/Kaufman assay) (92, 95) or by DTT (Shiman assay) (31).

posing a catalytic core) but not by phosphorylation. Under these conditions, for example, PAH will hydroxylate tryptophan at the same 5-position as TrpH (13, 14).

The PAH active site is of additional interest in that it is able to perform the same spectrum of chemical transformations as cytochrome P450 without benefit of a heme prosthetic group (15–17). A variety of other transformations of isosteric amino acids is possible, including epoxidation, aliphatic hydroxylation, and the formation of nitrogen and sulfur oxides (15–17). In contrast to the microsomal hydroxylases, PAH activity is tightly regulated at the post-translational as well as transcriptional level, and its oxidative chemistry is much more specific.

The molecular genetics of phenylalanine hydroxylase have been of intense interest ever since the human gene was located (18) because of the molecular nature of PKU, the possibility of preparing vectors for gene therapy (19), and the ability to prepare PKU-mutant proteins in an effort to link genotype and phenotype (20). Using heterologous expression followed by activity assays of cell lysate, various PKU mutations have been associated with unstable mRNA, unstable/unfolded proteins, or apparently intact proteins that have low activity (21). In the last case, the specific origin of the molecular defect in the complicated activation and catalytic pathways of PAH cannot be determined until the protein is purified to homogeneity and compared with a thoroughly characterized wild-type PAH. The dissection of this process into discrete, fully characterized steps and structures is essential for determining both the mechanism of catalysis and ultimately the chemical basis of PKU, but it has not yet been possible because of the heterogeneity of the protein. For instance, the observation of PKU due to diminished sensitivity to L-Phe might be due to either a decreased active site or allosteric site L-Phe affinity, or it might result from improper phosphorylation, subunit assembly, allosteric interactions, *etc.*

We have embarked upon a research program involving detailed spectroscopic and mechanistic characterization of PAH, with special attention to the active site iron's properties. No previous method of preparing PAH from rat liver tissue or a recombinant source is suitable for the purification of the large amounts (>100 mg) of spectroscopically homogeneous material that we require. PAH isolated from rat liver is a mixture of alleles, having variable levels of phosphate and different types of tightly bound iron (3). Recombinant PAH expressed in baculovirus is fully phosphorylated and highly active but would be expensive to manufacture on a large scale (22). Prokaryotic expression has the potential to provide sufficient quantities of enzyme but has not yet been optimized for yield, iron content, and purity or characterized in sufficient detail. To establish a base line from which we can reliably compare different states and forms of the enzyme, we report an efficient, large-scale expression of rat hepatic PAH in *Escherichia coli* and a comprehensive set of its kinetic and spectroscopic properties.

The large (~34 kcal/mol) (3) Arrhenius activation barrier to the T → R conversion suggests that significant structural distortions of the PAH tetramer occur during allosteric activation. It is not known if the alterations are largely protein-centered or are caused by a change in the coordination environment of the essential active site iron. Using a combination of spectroscopic probes of this process, we show that the direct effects activation has on the active site configuration are limited, while prominent changes occur at the tertiary/quaternary levels of protein structure. The steady state properties of the R state active site, across an unprecedentedly broad range of substrate concentrations, indicate sequential binding of L-Phe, 6-MPH_4, and O_2 prior to catalytic steps. We introduce a novel adduct of reduced PAH and NO, which models the interaction of Fe^{2+} and O_2 at the active site and can be used as a structural probe of that complex. A model based on metal-centered, biophysical, and kinetic observations of recombinant PAH is presented to explain the reactivity properties of the enzyme in terms of the T → R transition.

EXPERIMENTAL PROCEDURES

Materials—The PRPH3 clone containing a full-length cDNA of rat hepatic PAH was a gift of R. G. H. Cotton and H.-H. M. Dahl (23). The PKKT7(-E) protein expression vector and host strains JM105 and BL21(DE3) were gifts of S. Schultz and T. Steitz (Yale University). Polyclonal sheep anti-PAH antibody was the gift of J. Tipper and S. Kaufman (National Institutes of Health) (24). Bovine liver catalase, bovine erythrocyte superoxide dismutase, goat anti-sheep IgG/alkaline phosphatase conjugate, L-Phe, MOPS, phosphates, salts, glycerol, and molecular weight markers were obtained from Sigma. Ampicillin, isopropyl-1-thio-β-D-galactopyranoside, and DTT were obtained from U. S. Biochemical Corp. Phenyl-Sepharose CL-4B was obtained from Pharmacia (Uppsala, Sweden). 6-MPH_4 was synthesized by standard methods (25, 26) and was stored at −20 °C until use. Induced cells and purified recombinant PAH (rPAH) were stored at −70 °C. All DNA-modifying enzymes were obtained from New England Biolabs or U. S. Biochemical Corp. All other reagents and solvents used were of reagent grade.

Construction of Plasmid Vector—Oligonucleotides were synthesized complementary to the 5′- and 3′-ends of the desired coding regions of PRPH3, with non-annealing tails containing *Eco*RI and *Sal*I sites, respectively, immediately adjacent to the PAH-derived sequence. These were used as polymerase chain reaction primers with the linearized cDNA clone PRPH3 as template. The amplified product was then cloned into the *Eco*RI-*Sal*I sites of PKKT7(-E), which contains the ϕ10 RNA transcription start site recognized by T7 RNA polymerase (27), as well as a Shine-Delgarno sequence at −9 with respect to the initiator Met codon. The DNA sequence of expression construct in the region encoding rPAH was obtained from both strands by automated DNA sequencing. Standard molecular biological techniques were used for all of the above (28).

Growth and Induction of BL21(DE3) Cells—A glycerol stock of

BL21(DE3) cells (29) transformed by the method of Hanahan (30) was used as the source of protein-producing cultures. These were grown to an A_{550} = 1 in BMB broth (described below) at 50 μg/ml ampicillin and induced with 0.4 mM isopropyl-1-thio-β-D-galactopyranoside for 6 h at 30 °C in a New Brunswick Instruments fermentor before harvesting. The pH was maintained at 7.6 during the course of the growth, as was vigorous aeration. Antifoam A concentrate was added as necessary. Cells were pelleted at 7500 rpm for 10 min at 4 °C. Pellets were resuspended in an equal volume of lysis buffer (30 mM Tris, pH 7.25, 5 °C, 0.2 M KCl, 80 mM L-Phe), frozen in liquid nitrogen, and stored at −70 °C until protein was purified. Typically, 12–14 g/liter medium of cells are obtained in a 10-liter growth. BMB is a broth adapted from a BL21(DE3) medium developed by Craig Martin (University of Massachusetts). It contains Bacto-tryptone (1% w/v), dextrose (2% w/v), NH_4Cl (100 mM), phosphate (60 mM, pH 7.8), NaCl (10 mM), $MgSO_4$ (2 mM), $CaCl_2$ (100 μM), H_2BO_3 (12 μM), $FeCl_3$ (25 μM), Na_2MoO_4 (8 μM), and KI (6 μM). Immediately before the introduction of bacterial cultures, all components were mixed from separate sterile stocks. The iron stock was prepared freshly in 5 mM HCl.

Purification of rPAH—A method adapted from that of Shiman *et al.* (31, 32) was used to isolate rPAH from induced *E. coli* cultures. Following sonication of the thawed cell suspension, the lysate was spun 20 min at 18,500 rpm. The supernatant was heated to 25 °C and maintained at this temperature for a further 10 min to activate PAH. After clarification by centrifugation (20 min at 18,500 rpm), the supernatant was applied to phenyl-Sepharose CL-4B at 4 bed volumes/h as described by Shiman (32). Subsequent washes were carried out as has been described, but the buffer A with 5% *N*,*N*-dimethylformamide and buffer B washes were carried out at 6 bed volumes/h. Elution with buffer C was also performed as described, except that the second phenyl-Sepharose column was omitted, and the eluate was concentrated directly on a bed of pre-equilibrated DE-52 resin (5 mg rPAH/ml column volume). Following the DE-52 wash and 0.3 M KCl bump steps, the pure rPAH was concentrated to ≤1 ml using either a Centriprep 30 device or ultrafiltration on a YM30 membrane (both Amicon). At this point, the enzyme was judged to be >95% pure, but if further purification was required, up to 20 mg of rPAH was purified by applying it to a Pharmacia Mono Q 5/5 column (at ≤50 mM KCl), from which a linear gradient between 0 and 300 mM KCl was used to elute essentially homogeneous protein. In some situations, up to 50 mg of purified protein was applied to a Superdex 200 26/60 column (Pharmacia) and eluted with 20 mM phosphate buffer at pH 6.0.

Generally the purifications do not include an iron-addition step. When this step was performed, catalase (2,000 units/ml) and superoxide dismutase (10 units/ml) were added to the supernatant between the first spin and the L-Phe activation step. After 1 min at 25 °C, the lysate was made 5 mM in DTT and 0.75 mM in $Fe(NH_4)_4(SO_4)_2$, followed by the second spin and subsequent purification steps.

Assays—PAH activity was determined using the standard assay, in which the formation of tyrosine from 1 mM L-Phe (in the presence of 60 μM 6-MPH_4 and 6 mM DTT) is monitored at 275 nm in 0.1 M phosphate with 3000 units/ml catalase (33). For the determination of kinetic constants, PAH was preincubated at 25 °C with either 1 mM L-Phe for 3 min or 0.5 mM lysolecithin for 5 min. Activated enzyme (5 μg/ml at a specific activity of 6 units/mg, where 1 unit = 1 μmol of Tyr formed min^{-1}) was added as the last ingredient to a complete assay mixture whose initial velocity was determined, either from the slope of the first 30 s or by direct simulation of the data.

Determinations of L-Phe or lysolecithin activation at equilibrium were carried out as described (33). Briefly, 20 μl at the indicated [activator], containing 10 μg of enzyme, was preincubated for 5 min at 25 °C and then added as the last ingredient to a standard assay mix at 11 °C. The lower temperature is necessary to minimize further activation by 1 mM L-Phe. No significant variation in the initial slope was observed over the first 30 s of reaction, which was the interval used for velocity determinations.

For activity assays performed using stopped-flow detection, the reagents are loaded into two syringes; the first syringe contains rPAH (±L-Phe) in phosphate buffer, and the second syringe contains pterin, DTT, and L-Phe in a modification of a previously reported procedure (34). The solutions are preincubated 5 min at 25 °C, loaded into syringes, and equilibrated at the desired assay temperature for 10 min before the first of several injections. Stopped-flow assays show a lag in the first few seconds of assay due to the obligate prereduction of rPAH, which could be avoided by the addition of up to 20 equivalents of 6-MPH_4 to the enzyme-containing syringe.

Observation of the *q*-6-MPH_2 formed by reduction of rPAH was carried out at 334 nm, where the formation of *q*-6-MPH_2 results in an increased absorbance (at this wavelength, the molar absorptivities of 6-MPH_4 and 6-MPH_2 are equal and lower than that of *q*-6-MPH_2). In these assays, DTT is omitted, and pterin is added as the last ingredient to an otherwise complete assay mix at pH 8.0 exactly as described. Under these conditions, the 4a-carbinolamine form of 6-MPH_2 (4a-hydroxy-6-MPH_2) that is the initial product of the *catalytic* cycle dehydrates slowly to *q*-6-MPH_2, and so the initial product can be identified for each reaction (7).

Analytical Methods—Routine analytical procedures, including SDS-PAGE and Western blotting, were performed as described in standard handbooks (28). Protein quantitation was carried out using the Bradford method using bovine serum albumin as a standard, according to the manufacturer's instructions (Bio-Rad). These values were confirmed with total amino acid analyses performed by the Keck Biotechnology Center of the Yale Medical School. A prepacked Superdex 200 26/60 column (Pharmacia) was used for preparative as well as analytical gel filtration.

Phosphate Incorporation—In a typical experiment, 0.1 mg of rPAH (2 nmol) is treated with 4 μg of cAMP-dependent protein kinase (Sigma, 5 pmol units) in a total volume of 37.5 μl containing the following: 13.5 nmol of [γ-^{32}P]ATP (3 μCi total), 0.38 nmol of cAMP, 0.38 nmol of magnesium acetate, 0.75 nmol of DTT, 0.75 nmol of NaF, and 0.75 nmol of potassium phosphate at pH 6.8. A control reaction containing 26.7 μg of histones (2 nmol total, Sigma Type VI-S/H 6881) was run in parallel at 30 °C. Aliquots of 5 μl were withdrawn at different times, mixed into an equal volume of 2 × SDS gel dyes, and frozen in liquid N_2. These samples were heated to 100 °C for 5 min before loading a known fraction of the radioactivity onto a 20% acrylamide gel. Under these conditions, free label is well separated from protein in a "dry" blot of the gel. The radioactivity comigrating with each of the proteins was quantitated on a Betagen (Waltham, MA) Betascope 603 Blot Analyzer.

Other Methods—UV/visible spectra and kinetic measurements were obtained on a Perkin-Elmer Lambda 6 spectrophotometer. Stopped-flow work was performed on a Applied Photophysics DX.17MV sequential stopped-flow spectrometer (Leatherhead, United Kingdom). Fluorescence measurements were acquired on a Spex FluoroMax. Atomic absorption was carried out with a Varian SpectrAA-20. EPR spectra were obtained on a homebuilt spectrometer interfaced to a Macintosh IIx computer (35). Sample temperatures were determined by calibration with a silicon diode thermocouple located immediately below the sample position. EPR samples of PAH ranged from 0.45 to 0.75 mM in iron and contained 50 mM MOPS, pH 7.2 (5 °C), with 300 mM KCl. The NO adduct of 6-MPH_4-reduced PAH (0.15 mM PAH, 100 mM MOPS, pH 7.2 (5 °C), 50 mM KCl) was obtained by the sequential addition of sodium dithionite and sodium nitrite under strict anaerobic conditions according to published procedures (36). Concentrations of the PAH-NO adduct were estimated by double integration of the EPR spectrum and comparison with the integrated EPR spectrum of a known concentration of Fe^{2+}·EDTA·NO prepared by literature methods (37). Conversions of approximately 85% were routinely obtained. Experimental conditions are described in the figure legends. CD spectra were obtained on an AVIV 62 DS. Dynamic light scattering data were obtained on a DynaPro 801 (Protein Solutions, Inc., Charlottesville, VA). Analytical small-zone gel filtration experiments were performed on a Pharmacia Superdex 200 26/60 column. Globular size standards used for determining the Stokes radius by gel filtration were apoferritin, catalase, alcohol dehydrogenase, bovine serum albumin, and carbonic anhydrase (38).

Data Analysis—Catechol titration data were least-squares fit to the following expression:

$$\Delta\text{Abs} = \frac{(C + E_a + K^{-1}) - \sqrt{(C + E_a + K^{-1})^2 - 4CE_a}}{2\varepsilon} \qquad \text{(Eq. 1)}$$

and solved as a function of C for K and ϵ (where C = concentration of catechol, E_a = concentration of enzyme containing active iron, K = catechol·rPAH complex dissociation constant, and ϵ = complex molar extinction coefficient). Steady state kinetics double-reciprocal analysis was done using Mathematica (Wolfram Research) using the sequential mechanism velocity expression:

$$\frac{1}{v} = \frac{K_{\text{phe}}}{V[\text{phe}]}\left[1 + \frac{K_{i,\text{phe}}K_{6-\text{MPH}_4}}{K_{\text{phe}}[6\text{-MPH}_4]}\right] + \frac{1}{V}\left[1 + \frac{K_{6-\text{MPH}_4}}{[6\text{-MPH}_4]}\right] \qquad \text{(Eq. 2)}$$

where v = initial velocity, V = maximum velocity, K_x and $K_{i,x}$ are the Michaelis and dissociation constants for species x, respectively. Data were weighted as the square of the velocities (39). Routine analyses were performed with KaleidaGraph (Abelbeck Software). Analysis of transient kinetics was carried out using the Kinsim/Fitsim software

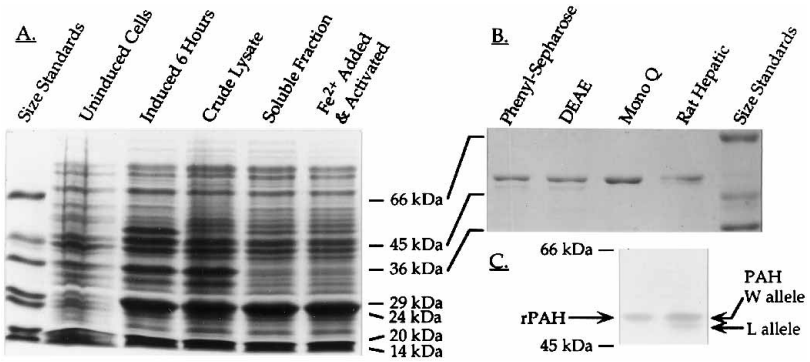

FIG. 2. *A*, purification of rPAH. *Lanes 1–5* contain 20 μg of protein from the indicated purification steps (see Table I). *Lanes 5–7* contain 2 μg of protein. *B*, purification of rPAH to homogeneity. Each *lane* contains 2 μg of protein at the indicated stage of purification. Also shown is rPAH purified through the Mono Q step (see "Experimental Procedures"). *C*, Western blot of 1 μg of protein, developed using a polyclonal antibody to PAH. The functionally similar "W" and "L" alleles can be distinguished in the rat hepatic PAH lane, whereas the rPAH shows only the "W" allele, as expected. Size standard positions are indicated.

package by C. Frieden and co-workers (40, 41), rewritten by G. Mudunuri (Texas A & M, College Station) for use on a Silicon Graphics workstation. The kinetic mechanism used in simulations was that employed by Shiman and Gray (33), in which the L-Phe activation and iron site inactivation are treated as sequential first-order processes.

RESULTS

Overexpression and Purification of rPAH—The plasmid described here is compatible with the T7 RNA polymerase-coupled systems developed by Studier and co-workers (29) for high level protein expression. The DNA sequence from both strands of the region encoding rPAH was obtained and found to match the protein-coding region sequence reported by Dahl and Mercer (23) with the exception of codon 87, which was found to be AGC (Ser) rather than the expected ACG (Thr). Ser is found at this position in the extremely similar mouse PAH (442/452 amino acid identity, 98%), in an area of the protein thought to be of regulatory rather than catalytic importance. PAH activity detected in the crude lysate of induced cultures increases over 6 h, in register with the appearance of a soluble M_r = 51,000 protein in SDS-PAGE. The optical density of induced cultures continues to increase slightly, which suggests that PAH induction is not particularly toxic to the cells. Maximum amounts of soluble rPAH were obtained from inductions at 30 °C, yielding ~90 mg of purified rPAH from a 10-liter fermentor growth (Fig. 2).

Direct adaptation of the purification scheme of Shiman *et al.* (32) for the scale described above resulted in rPAH of activity 7 ± 1 units/mg; purification of protein from two combined 10-liter growths is described in Table I. Recombinant PAH is isolated with specific activity and activation behavior essentially identical to that of enzyme from rat liver. The phenyl-Sepharose-based purification procedure requires that rPAH undergo a reversible, L-Phe-induced increase in hydrophobicity. This affords a purification from incorrectly assembled forms of PAH, some of which may have enzyme activity, thereby lowering the apparent recovery.

The expression of the rat hepatic PAH cDNA in *E. coli* is correlated with the appearance of a M_r = 51,000 protein that cross-reacts with a polyclonal antibody to rat hepatic PAH in a Western blot. Only full-length protein is purified by this procedure, despite the observation of small amounts of a cross-reactive 47-kDa protein observed in soluble cell lysate (data not shown). The electrophoretic mobility of rPAH is identical to that of the rat "W" allele, from which the cDNA clone was obtained. Under SDS-PAGE conditions, the minor "I" allele (Ile-371 rather than Thr-371) is resolved at a slightly smaller apparent M_r (≈49,000). Total amino acid analysis was performed on the recombinant protein, which was found to agree well with the predicted protein sequence. An extinction coefficient for rPAH could be calculated upon this basis: a 1 mg/ml solution at 25 °C in 0.12 M phosphate, pH 6.8, gives rise to an absorbance of 1.05 at 280 nm and gives an apparent Bradford reading of 1.05 mg/ml.

The relatively strong induction of rPAH (on the order of 5% total bacterial protein) allowed the deletion of several items from the standard purification, among them the use of Tween 80 and the use of a second, smaller phenyl-Sepharose column. PAH from rat liver is generally purified with an iron addition step, resulting in stoichiometric amounts of iron and improved activity. The conditions used for iron addition, which involve the addition of ferrous iron to oxygenated buffers in the presence of reductant, are associated with the generation of reactive oxygen species that might damage PAH. Inclusion of enzymes known to scavenge reduced, reactive oxygen species improved the specific activity of the protein purified with an iron addition step from 5 to 8 units/mg.[2] Whether this observed increase in specific activity results from the degradation of peroxide or superoxide, or by some other mechanism, is unknown. In general, purifications including an iron addition step did not result in rPAH of higher specific activity despite the observation of more iron per subunit in treated protein. This has also been observed with partially purified rat hepatic enzyme (42). Omission of this step altogether results in protein containing near stoichiometric levels of iron (0.7 iron/subunit), with specific activity that depends directly on iron content. This implies that there is very little protein containing inactive iron. This *fractional* specific activity is consistently 10.5 ± 0.5 units/mg per 1 catalytically competent iron atom/subunit.

Demonstration of Stoichiometric Phosphorylation—Using a modification of previous procedures, we found that T state rPAH is a good substrate for cAMP-dependent protein kinase. The reaction is essentially complete after a 30-min exposure to conditions that phosphorylate Ser-16 (hepatic protein numbering). Unlike previous reports concerning rat hepatic PAH phosphate content, rPAH as isolated appears to be unphosphorylated at this critical residue. In comparison to a saturated histone standard, rPAH incorporates 0.97 ± 0.05 phosphate per subunit (average after 30 min), indicating that initially it was completely unphosphorylated. The reason for this discrepancy with a previous overexpression in *E. coli*, in which 0.1–0.2 phosphate per subunit was determined, is unknown. These investigators quantitated total protein-associated phosphate

[2] Although large amounts of catalase are added, neither this nor superoxide dismutase appears to copurify with rPAH as estimated by SDS-PAGE.

TABLE I
Purification of rPAH from E. coli

Velocities from the standard assay are at 1 mM [L-Phe]. Protein was quantitated by the Bradford method. Final overall 20-fold purification from ~200 g of wet cells.

Purification step	Volume	Activity[a]	Protein	Specific activity	Yield
	ml	*units*	*mg*	*units/mg*	%
Total cell lysate	705	2470	22,800	0.11	
Soluble fraction	515	4940	14,400	0.34	100
Activated/Fe^{2+}[b]	510	4490	12,400	0.36	91
ϕ-Sepharose elution	490	830	122	7.0	17
DEAE concentrated	65	910	134	6.8	18

[a] One unit = 1 μmol tyrosine formed min^{-1} mg^{-1}.
[b] The iron addition step does not increase rPAH yield or activity.

(43), whereas our assay is specific for the regulatory phosphorylation site.

rPAH Hydrodynamic Properties—Proper assembly of PAH subunits into a tetrameric structure is an essential prerequisite for allosteric activation behavior. Gel filtration experiments performed at relatively high rPAH concentrations (>0.4 mM subunit) confirm that rPAH adopts a structure that elutes at a position consistent with a tetramer both in the absence (apparent molecular mass for PAH^T, 248 kDa) and presence (apparent molecular mass for PAH^R, 270 kDa) of the allosteric activator L-Phe. In analogous studies performed with lower concentrations of homogeneous enzyme (<0.1 mM subunit), a peak corresponding to a dimer of rPAH is observed (apparent molecular mass for PAH^T, 120 kDa). The distribution of rPAH oligomeric species systematically shifts from tetramer to dimer as the pH of the phosphate elution buffer is increased (Fig. 3). While only qualitative information can be obtained from small-zone gel filtration studies (44), the observation of distinct bands demonstrates that the self-association of dimers is slow on the time scale of the separation. In parallel experiments, the addition of 0.5 M KCl causes a ~10% increase in the proportion of dimer at pH 6.8 but leaves the distribution unchanged at pH 8.0. R state rPAH, generated by prior incubation at 25 °C with L-Phe and eluted over the column in buffer supplemented with 1 mM L-Phe, shows a greater propensity to remain tetrameric. The addition of 0.5 M KCl to $rPAH^R$ (at either pH 6.8 or 8.0) does not perturb the oligomeric distribution. These observations may bear some relationship to the pH dependence of the obligatory activation phenomenon, which is several times faster at higher pH (pH = 9) than at neutrality and possibly even to the quaternary rearrangement underlying the allosteric transition (45). Using a calibration curve of the known Stokes radii of several gel filtration standards, Stokes radii could be estimated from gel filtration retention times: $rPAH^T$ = 55 Å and $rPAH^R$ = 57 Å. These values agree well with the reported value of 55 Å determined by gel filtration for partially phosphorylated resting state rat hepatic PAH (46). While a detailed description of the structural changes induced by the $rPAH^T$ to $rPAH^R$ conversion and its effect on the catalytic iron site is still under investigation, the observed ~10% increase in the volume of rPAH following activation is consistent with the high apparent Arrhenius activation energy for this process of ≈35 kcal/mol (3).

These conclusions are supported by data obtained from dynamic light-scattering studies. The relatively narrow dynamic range of this experiment limited studies to 5 mg/ml rPAH (0.1 mM subunits in 0.1 M phosphate buffer). At this concentration, the Stokes radius observed for $rPAH^T$ was 51 ± 2 Å. The same values are obtained at pH 6.0, 8.0, and at pH 8.0 with 0.5 M KCl present. Unfortunately, data from $rPAH^R$ samples were unreliable, apparently because of aggregation.

Optical Spectroscopic Characterization—As with the optical spectrum of rat hepatic enzyme, both ferric $rPAH^T$ and $rPAH^R$ show broad absorbances in the near-ultraviolet and visible spectral regions (300–400 nm; ϵ_{330} = 3,000 M^{-1} cm^{-1}) with a trailing absorbance that extends beyond 500 nm (Fig. 4).[3] These features, which are absent in optical spectra of both the apoprotein and reduced holoenzyme, have been assigned as arising from histidine-to-Fe^{3+} ligand-to-metal charge-transfer (LMCT) transitions. Analogous His-to-Fe^{3+} LMCT transitions have been reported for the crystallographically characterized non-heme ferric metalloenzymes soybean lipoxygenase (ϵ_{330} = 1500 M^{-1} cm^{-1}) (47, 48) and superoxide dismutase from *E. coli* (ϵ_{350} = 1850 and 1675 M^{-1} cm^{-1}) (49–51). Although contributions from similar transitions involving carboxylate ligands

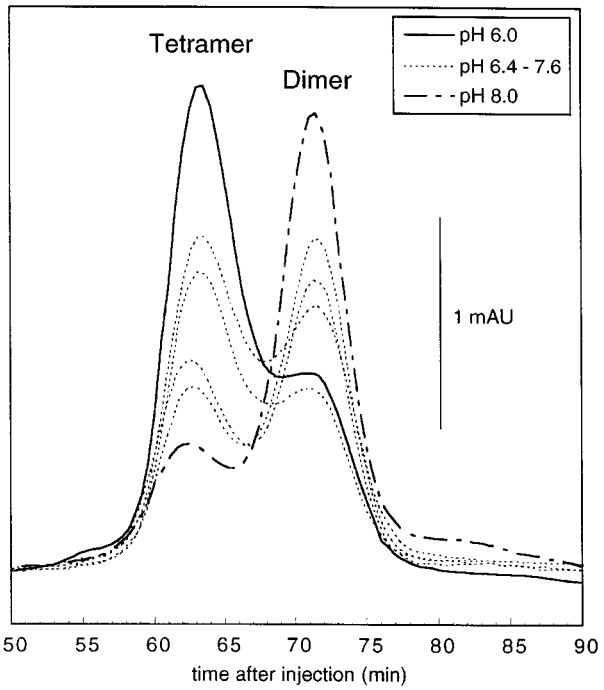

FIG. 3. **Dissociation of rPAH tetramers into dimers as the pH is increased, detected by small-zone analytical gel filtration monitored at 280 nm.** A Superdex 200 26/600 column was eluted at 2.5 ml/min with 0.12 M phosphate at 5 °C, at pH 6.0, 6.4, 6.8, 7.2, 7.6, and 8.0 (ionic strengths ranged from 86 to 122 $mohm^{-1}$ cm^{-1}). A common stock of rPAH was prepared by purifying 30 mg of rPAH over Superdex 200 at pH 6.0. A conservative cut from the tetramer peak was saved for rechromatography, excluding aggregate, oligomer, and dimer fractions. Each injection was of 200 μg of rPAH diluted freshly 38-fold in the elution buffer (~4 μM [subunit] at t = 0); all elutions were done on a single day to avoid artifacts due to freeze-thaw cycles. Chart-recorder traces were manually digitized using Mathematica. The data presented have not been corrected for small variations in the amounts of rPAH injected.

[3] E. Glasfeld, Y. M. Xia, P. G. Debrunner, and J. P. Caradonna, submitted for publication.

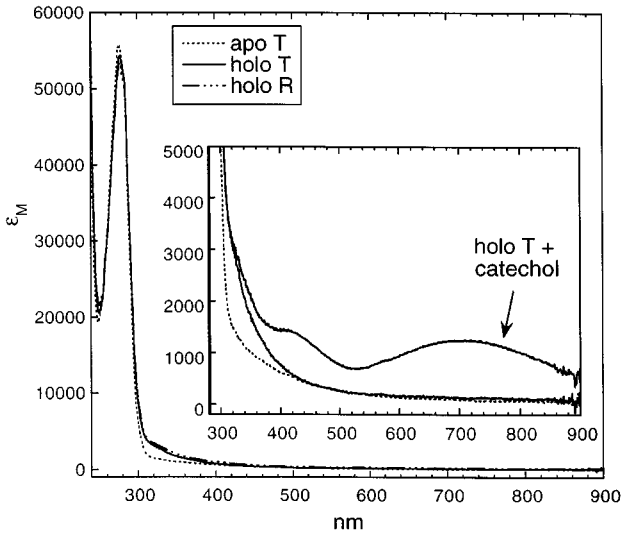

FIG. 4. **Spectra of ferric rPAH$^{T/R}$ and iron-depleted (apo) rPAH^T at 25 °C.** The holoenzyme T/R spectra were obtained in 50 mM MOPS, 0.3 M KCl (pH 7.3) at 25 °C. R state enzyme was generated from T state by addition of L-Phe to 1 mM followed by a 5-min incubation at 25 °C. The contribution from buffer and for the R state spectra, L-Phe, has been subtracted. The apoprotein sample was prepared by treating 2 mg of rPAH (specific activity, 6.0 units/mg, 0.9 iron/subunit) with 1 mM *o*-phenanthroline and 1 μl of 10% β-mercaptoethanol in a total volume of 250 μl. The increase at 510 nm due to the formation of $[Fe(o\text{-phen})_3]^{2+}$ was monitored at 25 °C for 60 min, by which time ≥94% of the iron had been removed. Small molecules were removed by passage over a column (0.8 × 6.3 cm) of Sephadex G25 (medium grade, Pharmacia) equilibrated in 0.1 M phosphate, 5% glycerol buffer (pH 6.8). Glycerol is present to stabilize the apoprotein and facilitate gel filtration, but it tends to exaggerate the molar absorptivity of PAH. A control holoenzyme rPAH^T sample that was exchanged into the same 5% glycerol buffer shows a ~15% more intense absorbance at 280 nm and stronger absorptions above 290 nm. *Inset*, difference spectrum showing new chromophores formed upon incubation of ferric rPAH^T with catechol. 20 equivalents of catechol were added to 1.06 mg of rPAH^T (specific activity, 5.3 units/mg, 0.96 iron/subunit) in a final volume of 0.8 ml in 50 mM MOPS, 0.3 M KCl (pH 7.3) at 25 °C. Using ϵ_{698} = 1900 M^{-1} cm^{-1} determined by active site titrations (described in text), 15 μM of the catechol-Fe^{3+} adduct forms (subunit concentration = 25.7 μM), indicating that the fraction of "active" iron is 0.58. Uncomplexed catechol does not absorb above 400 nm under these conditions (data not shown), and its contribution has not been subtracted from the spectrum. Catechol stocks were standardized in methanol, using ϵ_{277} = 2700 M^{-1} cm^{-1} (Sadtler Research Laboratories, Ultra Violet Spectra 108 UV, Philadelphia).

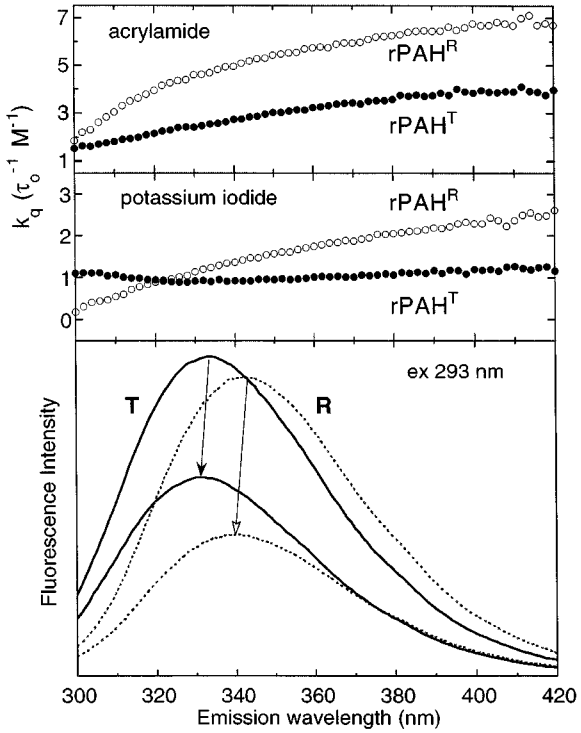

FIG. 5. **Fluorescence emission spectra at 25 °C of 70 μg/ml ferric rPAH$^{T/R}$ (1.4 μM subunits) in 0.1 M phosphate buffer, pH 6.8, activated where indicated with 10 mM L-Phe.** Samples were purified over Superdex 200 to remove small molecules. Spectra were recorded with vigorous stirring and are corrected for dilution. Excitation wavelength was at 293 nm with a 2-nm slit width, while emission slit width was 4 nm. Also shown is the effect of quenching of each by 0.2 M acrylamide. *Top*, Stern-Volmer plots of quenching due to acrylamide (5 values between 0 and 0.2 M) or potassium iodide (5 values between 0 and 0.4 M). The T state is represented by a *solid line* and *filled circles*, and the R state is represented by a *dotted line* and *open circles*.

cannot at present be eliminated from discussion, the lack of any LMCT transitions characteristic of tyrosinate-to-Fe^{3+}, cysteinate-to-Fe^{3+}, or inorganic sulfide-to-Fe^{3+} charge-transfer transitions in the visible spectrum allows the elimination of these groups as potential ligands to the active site iron. Thus, the optical spectrum of ferric rPAH is consistent with the presence of coordinated histidine as well as oxygen atom donors such as carboxylates and/or water.

The fluorescence spectrum of PAH is dominated by the characteristic emission of three tryptophans, which can be selectively excited at 293 nm (Fig. 5). The fluorescence emission of activated rPAH is red-shifted relative to resting enzyme, which is also typical of rat hepatic enzyme (52, 53). In addition, the rPAH^R fluorescence is more susceptible than that of rPAH^T to quenching by small molecules, whether anionic or neutral. Quenching of the protein fluorescence by acrylamide or by potassium iodide yielded Stern-Volmer plots analogous to those using comparable concentrations of free tryptophan. This is interpreted as an indication that the fluorophore exposed upon activation behaves as if it were a single tryptophan moving closer to bulk solvent (53). These observations are also consistent with the observed increase in hydrophobicity upon activation that is exploited in the purification procedure.

The CD spectra of T (Fe^{3+} and Fe^{2+}) and R (Fe^{3+} and Fe^{2+}) states of rPAH (Fig. 6), obtained at 4 μM [subunit] from 400 to 195 nm, were found to be quite similar (Table II). These spectra were analyzed with a standard basis set to estimate a linear combination of four structural elements, assuming a mean helix length of 10 residues (54). There appears to be a slightly increased fraction of helix in the R state samples compared to T state. Overall, significantly greater helical content was predicted than has been reported elsewhere for PAH, while the distribution of random coil predicted is quite small compared to a previous report. We report data to lower wavelengths (195 nm *versus* 210 nm) critical to the assignment of secondary structure, which might explain the discrepancy with earlier results (55).

Catechol Binding Studies—Catechol binds tightly to rPAH^T and rPAH^R containing a catalytically competent iron site, as determined by the appearance of an intense blue-green color arising from a catechol-to-Fe^{3+} LMCT band centered at 698 and 435 nm (Fig. 4) (56). As shown in Fig. 7, the addition of catechol to rPAH that contains both inactive and active iron (specific activity, 6 units/mg; 0.9 iron/subunit) reaches saturation at 0.6 equivalents of catechol per subunit, consistent with a fractional specific activity of 10.5 ± 0.5 units/mg. Catechol-active iron complex formation occurs with ϵ_{698} = 1900 M^{-1} cm^{-1} and $K_d = 3.6 \times 10^{-7}$ M, where the concentration refers to enzyme subunits containing active iron rather than total protein. A second higher energy LMCT band is observed at 435 nm ($\epsilon \approx 2000$ M^{-1} cm^{-1}). Enzyme samples at near-stoichiometric levels of iron per subunit that were allowed to inactivate on the

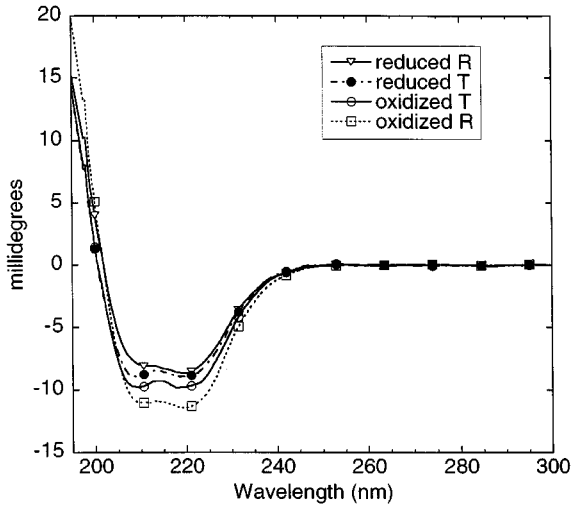

FIG. 6. **Circular dichroism spectra of oxidized/reduced rPAH$^{T/R}$ at 25 °C in 20 mM phosphate buffer, pH 6.8, with 0.1 M KCl, at 0.2 mg/ml rPAH (4 μM subunits).** Each of the T state samples was prepared by 2 min, 25 °C incubation of 24 nmol rPAH with either 48 nmol 6-MPH$_4$ or the equivalent volume of buffer (12 μl) in a total volume of 90 μl. Samples were made 0.1 M in KCl, passed over 2 ml P-10 (Bio-Rad) equilibrated in the same buffer, which was then used to elute protein free of pterin. R states were generated from these samples by addition of L-Phe to 1 mM, followed by a 5-min incubation at 25 °C to activate the enzyme. All spectra were obtained at 25 °C. Pathlength = 0.5 mm, scan rate = 0.5 nm/s, 5 scans averaged per spectrum. Spectra were base-line corrected using the average value of 250–300 nm as zero.

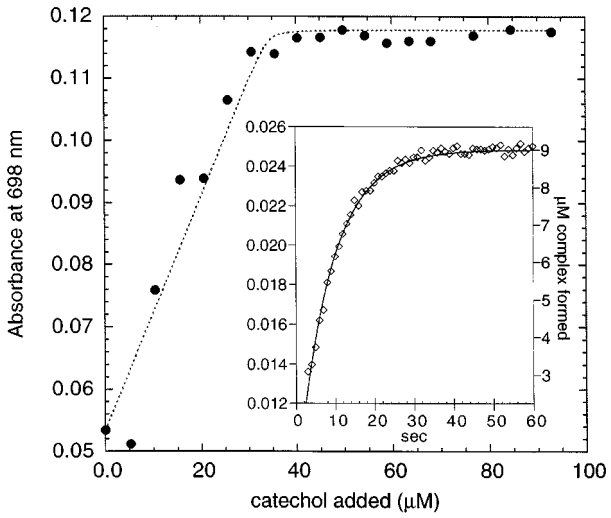

FIG. 7. **Catechol binding to active iron in 50 mM MOPS, 50 mM KCl (pH 6.8).** Absorbance at 698 nm plotted as a function of catechol titrated into a solution of rPAH at 3 mg/ml (60 μM subunits; specific activity, 6 units/mg; 35 μM active iron-containing subunits). Each point is the result of a 5-min, 10 °C incubation of rPAH at the indicated [catechol]. Titration data were fit to the expression given under "Experimental Procedures." *Inset*, binding of 11 μM catechol to 11 μM rPAH^T at 18 °C monitored at 698 nm in 50 mM MOPS, 0.3 M KCl (pH 7.3). The *solid line* is a simple first-order fit to the data with k_{obs} = 0.11 s^{-1}. Final chromophore corresponds to 9.0 μM, 8.8 μM expected from specific activity of 7.8 units/mg (102%).

TABLE II
Secondary structure predictions from circular dichroism spectra

Fits were performed on data from 250 to 195 nm, using the algorithm of Chang, *et al.* (54) to simulate the linear combination of four structural elements (α-helix, β-sheet, β-turn, and random coil) for each of the indicated states. Conditions are described in the legend to Fig. 6.

	α-Helix	β-Sheet	β-Turn	Coil
		%		
{Fe^{3+}} rPAH^T	28	41	4	27
{Fe^{2+}} rPAH^T	29	35	5	27
{Fe^{3+}} rPAH^R	35	38	5	22
{Fe^{2+}} rPAH^R	36	41	3	21

benchtop to 3 units/mg and 0.2 units/mg show correspondingly less intense absorbances at 698 nm following the addition of excess catechol. Since the catechol adducts of the catalytically competent Fe^{3+} sites of rPAH^T readily form with uncomplicated kinetics, these data suggest that some structural changes in the primary iron coordination sphere or protein tertiary structure during enzyme inactivation have eliminated access to the active iron center. Of further practical interest is the use of the relatively strong catecholate-to-Fe^{3+} LMCT transition, which appears in an uncluttered region of the optical spectrum, and the apparent selective binding of catechol to catalytically competent iron sites (*i.e.* not "inactive" iron, see "Discussion") as the basis of an active iron assay for PAH.

The visible spectra of the catechol adducts of ferric rPAH^T and rPAH^R are similar to a variety of mononuclear iron complexes (56). Data from model systems of similar coordination geometries containing ligands of varying Lewis basicities and charge indicate that the catecholate LMCT transitions are sensitive to the ligand environment and undergo a bathochromic shift as the net basicity of the ligands is decreased (56). As more highly charged oxyanionic ligands (carboxylates) interact strongly with the ferric center, the metal center's intrinsic Lewis acidity decreases, destabilizing metal *d*-orbitals relative to the filled catecholate orbitals thereby inducing a hypsochromic shift in the LMCT spectrum. Decreasing the basicity of the ligands (by exchanging carboxylate oxygen for N donors) would result in weaker metal-ligand interactions and a smaller catecholate-metal energy gap, which would induce a bathochromic shift in the LMCT spectrum. This effect can be quite dramatic with the low and high energy catecholate LMCT bands ranging from 800 and 495 nm (tris-(2-pyridylmethyl)amine) to 550 and 388 nm (*N*-(4,6-di-*tert*-butyl-2-hydroxybenzyl)-*N*-(carboxymethyl)glycine), with energy shifts of approximately 5700 cm^{-1} and 5550 cm^{-1}, respectively. While these data suggest that catecholate-to-Fe^{3+} LMCT transitions are sensitive probes of iron coordination environments, we are currently unable to satisfactorily deconvolute the overlapping contributions of ligand environment from factors such as solvent accessibility to active site, protein matrix environment (charge distribution, micro-dielectric constant) near the iron site, and hydrogen bonding networks that are known to induce significant shifts in the energy (1500–2000 cm^{-1}) of the LMCT bands for simple model complexes.

EPR Studies—The EPR spectrum of high spin ferric rPAH^T (Fig. 8*B*) in the noncoordinating MOPS buffer (pH = 6.8) is very similar to that reported for ferric rat hepatic PAH, consisting of broad axial features between 600 and 1400 G.[3] The broad EPR signals of resting state rPAH and hepatic PAH samples suggest that the iron domain maintains a distribution of conformations not due to factors known to induce heterogeneity in the rat hepatic enzyme (mixtures of active and inactive iron sites, presence of the T371I allelic variants, and variable levels of phosphorylation). This effect of micro-heterogeneity arising from slight perturbations in the symmetry of the iron coordination environment has also been noted in the EPR spectra of 4-hydroxyphenylpyruvate dioxygenase (57), the substrate complex of protocatechuate-3,4-dioxygenase (58), and transferrin (59, 60).

The electronic environment of the ferric center of rPAH^T is changed by small coordinating molecules such as Tris buffer. The axial EPR spectrum of rPAH in pH 6.8 Tris buffer (Fig. 8*A*) is significantly altered from the spectrum in MOPS buffer with two new signals appearing at g_{eff} = 6.7 and 5.4, giving the EPR

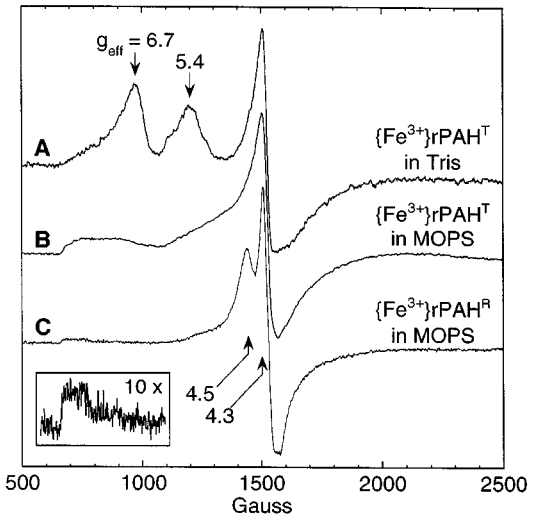

FIG. 8. *Spectra A* and *B* show EPR spectra of ferric rPAH^T (specific activity, 6 units/mg, 0.9 iron/subunit) obtained in Tris (*A*) and MOPS (*B*) buffers. In each case the buffer was 50 mM at pH 6.8 (5 °C). *Spectrum C* is the EPR spectrum of ferric rPAH^R (specific activity, 6.6 units/mg, 0.67 iron/subunit) obtained in 5 mM L-Phe, 50 mM MOPS, 0.3 M KCl (pH 7.2). This sample was activated at 1 mg/ml by incubating at 25 °C for 10 min and then concentrated by ultrafiltration over a YM30 membrane to 16 mg/ml. *Inset*, The rPAH^R lower Kramers' doublet at g_{eff} = 8.8. For *spectra A-C*, scan time = 12.8 min; sweep width = 2000 G; modulation amplitude = 20 G; modulation power = 3.6 μW; temperature = 4.3–4.4 K. Spectra are not to scale.

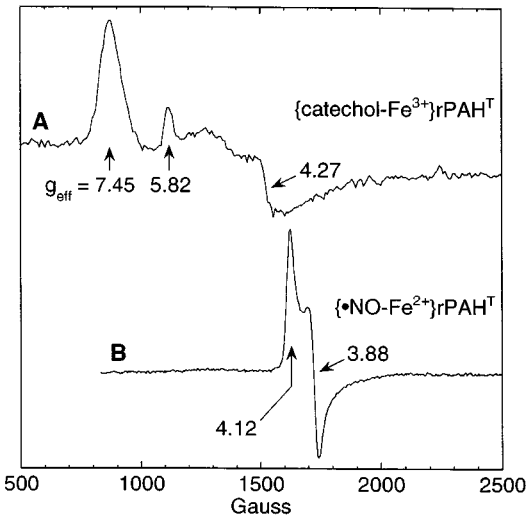

FIG. 9. *Spectrum A* is the EPR spectrum of the 1:1 adduct of rPAH^T (specific activity, 6.0 units/mg, 0.66 iron/subunit) with catechol (20-fold excess) obtained in 50 mM MOPS, 0.3 M KCl (pH 7.2). *Spectrum B* is the nitric oxide adduct of {Fe^{2+}} rPAH, which was prepared in an argon box under anaerobic conditions. 6-MPH$_4$-reduced rPAH (3.5 mg; specific activity, 8 units/mg; 0.7 iron/subunit) was diluted into 310 μl of degassed 100 mM MOPS, pH 7.3, with 50 mM KCl (three freeze-pump-thaw cycles). Small aliquots of degassed 0.1 M sodium ascorbate and 1 M $NaNO_2$ were added alternately in three rounds to a final volume of 1.4 ml. This was concentrated by centrifugation to 0.3 ml and loaded into the EPR tube, which was capped with a new septum. Estimation of the *E*/*D* for {FeNO}^{7} from the indicated crossing points was performed as described (93). All EPR samples were frozen slowly by suspension over liquid N_2, since a suitable glassing agent is unavailable for PAH (94). Both spectra were recorded with scan time 15 min; sweep width = 2000 G; modulation amplitude = 20 G; modulation power = 1.8 μW; temperature = 4.3–4.4 K. Spectra are not to scale.

spectrum previously reported for rat hepatic PAH (34, 59–61).

A significant change in the EPR spectrum is observed upon activation of ferric rPAH^T by L-Phe (Fig. 8*C*). The broad features observed in the rPAH^T spectrum are replaced by a new, prominent resonance at g_{eff} = 4.5 whose intensity decreases with decreasing rPAH specific activity, indicating that it is associated with the catalytically competent iron of rPAH. Activation significantly decreases the apparent micro-heterogeneity that is characteristic of the rPAH^T EPR spectrum, suggesting a tightening of the distribution of iron environments under these conditions. The electronic environment of the inactive iron at g_{eff} = 4.3 observed in both the rPAH^T and rPAH^R samples appears to be unaltered by the activation process. These data are equivalent to those observed for the rat hepatic enzyme.[3]

Non-activating exogenous ligands, in addition to Tris, sharpen the EPR resonances of rPAH^T. The spectrum of the 1:1 adduct of catechol and rPAH^T (Fig. 9*A*) indicates a complex with nearly axial environment with resonances at g_{eff} = 7.45 and 4.27 from the lower Kramers doublet and g_{eff} = 5.82 from the middle Kramers doublet, characteristic of an iron site with $E/D \approx 0.07$. It is not clear whether the catechol binds as a mono- or bidentate ligand, though resonance Raman studies were interpreted to support bidentate ligation (62). The spectrum resembles that obtained for bovine adrenal TyrH, which copurifies with a tightly bound catecholamine (63).

Ferrous PAH, which is the catalytically relevant form of the enzyme, is more refractory to spectroscopic study than the resting, ferric state of the enzyme. The modest Fe^{3+}-derived optical chromophores disappear, and high-spin Fe^{2+} (S = 1) becomes undetectable with standard EPR techniques, requiring specialized methods (Mössbauer, MCD, EXAFS) (64). The binding of nitric oxide, however, generates a yellow, EPR-active {FeNO}^{7} adduct (S = ½) with rPAH that will allow its use as a sensitive probe of the geometry and electronic properties of the ferrous active site (65, 66). The EPR spectrum of the nitric oxide complex of ferrous rPAH^T formed by exposure of the pterin-reduced enzyme to ascorbate/nitrite under anaerobic conditions is shown in Fig. 9*B*. This spectrum ($g_{y,x}$ = 4.12, $g_\perp$ = 3.88) is essentially identical to those reported for the NO adducts of isopenicillin *N*-synthase ($g_{y,x}$ = 4.09, $g_\perp$ = 3.95) (67), the non-heme iron site of photosystem II ($g_{y,x}$ = 4.09, $g_\perp$ = 3.95) (68), protocatechuate 4,5-dioxygenase ($g_{y,x}$ = 4.09, $g_\perp$ = 3.91) (69), catechol 2,3-dioxygenase ($g_{y,x}$ = 4.16, $g_\perp$ = 3.83) (37), soybean lipoxygenase (70), and the model complex [Fe(EDTA)(NO)]$^{2-}$ ($g_{y,x}$ = 4.10, $g_\perp$ = 3.90) (71). This signal originates from the ground state Kramers' doublet (M_s = ± ½) that resides on a center with S_T = ½. The two doublets (M_s = ± ½, ± ½) are split in energy by an amount Δ ($\Delta = 2D(1 + 3\lambda^2)^{1/2}$) in the absence of an external magnetic field. The parameter λ ($\lambda = E/D$) is a measure of the deviation from axial symmetry of the environment of the axial spin where D and E are the axial and rhombic zero-field splitting parameters, respectively. The value of λ may be determined under conditions in which $g_o\beta H \ll D$ and kT from the expression $g_{y,x} = g_\perp[1 + (1 \pm 3\lambda)/(1 + 3\lambda^2)^{1/2}]$ (37), yielding for rPAH at pH 7.3 $\lambda \approx 0.02$. Double integration of this spectrum *versus* a standard of [Fe(EDTA)(NO)]$^{2-}$ showed >85% conversion of enzyme bound iron to the NO adduct (data not shown). Furthermore, since the coordination of two NO molecules to the ferrous center is expected to yield an integer spin system having either no EPR spectrum or one significantly different from that shown in Fig. 9*B*, it is likely that only one iron coordination site is readily available for NO binding.

Obligate Prereduction of rPAH—Reduction of the enzyme, which is correlated with the ultimate reduction of the ferric center, is required for the formation of tyrosine. Physiological reduction is believed to be performed by the cofactor BH_4. rPAH reduction is accompanied by an increase in fluorescence and a decrease in the optical absorption in the LMCT region (similar to the apo spectrum in Fig. 4). Both enzyme reduction

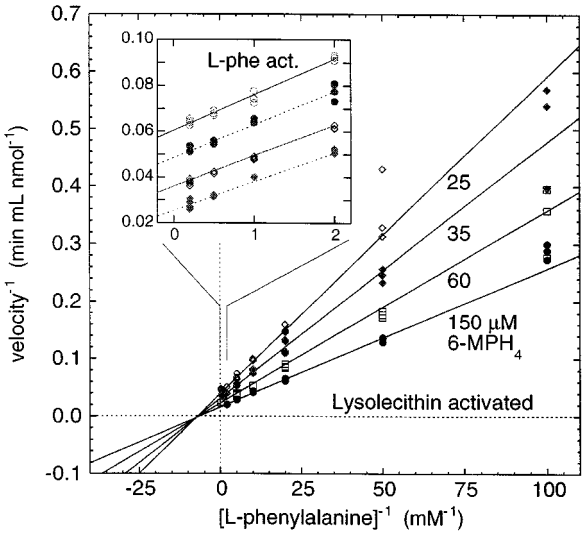

FIG. 10. **Double-reciprocal data determined with lysolecithin as activator, at saturating O_2 and fixed concentrations of 6-MPH$_4$.** Aliquots of rPAH^T were preincubated for 5 min in 0.5 mM lysolecithin (prepared freshly as a 4 mM stock in water) before the addition of DTT, L-Phe, and 6-MPH$_4$. L-Phe concentrations used ranged from 0.02 to 5 mM, and 6-MPH$_4$ concentrations ranged from 25 to 150 μM. At high [L-Phe], substrate inhibition occurred (see text). *Inset*, analogous determination with L-Phe as activator. Each was incubated at the given concentration of L-Phe for 10 min at 25 °C, which is sufficient to activate the enzyme fully. Initial velocities given are from assays that differ from the standard assay only by variation of each substrate's concentration.

and catalytic turnover produce *q*-6MPH$_2$ when 6-MPH$_4$ is used as cofactor, and in the case of reduction it is directly produced by the reaction. In contrast, the addition of 45 equivalents of 6-MPH$_4$ to 0.2 mg/ml oxidized rPAH^R in 1 mM L-Phe (18 °C, 0.1 M phosphate, pH 8.0) causes a ~1-min lag in the full velocity[4] of *q*-6-MPH$_2$ formation that is due to the slow nonenzymatic dehydration of 4a-hydroxy-6-MPH$_2$. Ferrous rPAH does not utilize the electrons derived from the reductant during the catalytic oxidation of substrate (7).

Enzyme Activation by L-Phe and Lysolecithin—Both rat hepatic PAH and rPAH display a requirement for preincubation with L-Phe to form or expose the PAH active site. The response of PAH activity to L-Phe indicates that it is a homotropic allosteric activator with a complex concentration dependence. Half-maximal equilibrium activation at pH 6.8 occurs at 0.11 mM Phe, compared with 0.12 for rat hepatic PAH (33). These data (not shown) may be replotted to give a Hill coefficient of 2.25, which is in an intermediate range of cooperativity. The Hill coefficient compares well to a previously reported value for rPAH (1.7) and to the various values reported for the rat hepatic enzyme (2.27–2.6) (43). We performed the same experiment on enzyme activated by lysolecithin, and found that the artificial activator gives rise to a similar fold stimulation in velocity with Hill coefficient 1.3 (data not shown). However, the distribution of oligomeric forms of lysolecithin-activated rPAH (as well as rat hepatic PAH) is unknown.

Initial Velocity Studies with L-Phe or Lysolecithin as Activator—Thorough preincubation with the substrate is a necessary condition for obtaining full activity under a given set of substrate concentrations (as well as a linear initial velocity trace). As a result, the range of L-Phe concentrations available for a double-reciprocal study is constrained between 0.4 and 5 mM, although slight substrate inhibition is observed at the highest [L-Phe] when [6-MPH$_4$] < 0.5 $K_{6\text{-MPH}_4}$. Kinetic constants were determined for rPAH over this narrow range (2.8–28 K_m) from a standard double-reciprocal set of experiments (*inset*, Fig. 10). The parallel appearance of the lines has been attributed to substrate saturation or inhibition rather than to a ping-pong mechanism. Using an expression for a sequential mechanism, one obtains K_{phe} = 0.37 mM (at 60 μM 6-MPH$_4$), $K_{6\text{-MPH}_4}$ = 38 μM (at 1 mM L-Phe), and $K_{i,phe}$ = 0.085 mM. The order of substrate addition is not known but is thought to be at least partially random (72).

TABLE III
Comparison of rPAH with rat hepatic PAH

Source	Rat liver, native[a]	*E. coli* overexpression
Max. iron/subunit	1.0	0.96
Typical phosphate content/subunit	0.2–0.3	<0.05
Hill coefficient (L-Phe activity)	2.6	2.25
V_{max} (units/mg)	8–14	6.8–8.8
$K_{app,pterin}$[b] (6-MPH$_4$)	45 μM	61 μM
$K_{app,phe}$ (6-MPH$_4$)[c]	0.18 mM	0.17 mM
{Fe^{3+} (catechol)} PAH complex	λ_{max} ≈ 700, 455 nm[d]	λ_{max} = 698, 435 nm
	ε_{700} = 1140 M^{-1} cm^{-1} *versus* [subunit]	ε_{700} = 1900 M^{-1} cm^{-1} *versus* [active iron]

[a] See Ref. 3.
[b] At 1 mM L-Phe.
[c] At 60 μM 6-MPH$_4$.
[d] Ref. 56. The specific activity is not stated for this sample, so the fraction of active iron is unknown.

To extend the range of the double-reciprocal plot, we used PAH activated with 0.5 mM lysolecithin, a structurally dissimilar, non-substrate activator. This allowed (Fig. 10) the determination of initial velocities at constant [rPAH] over a wide range of L-Phe concentrations, limited only by the sensitivity of the assay (useful between 5 and 35 nmol Tyr min^{-1} ml^{-1}) (31). The constants determined from this double-reciprocal plot are quite similar to those arising from the L-Phe-activated rPAH data, with the exception of K_{phe}, which is higher in the L-Phe-activated experiment. This provides further support that under standard steady state conditions, either L-Phe or lysolecithin activation results in a "functionally identical" state of the enzyme (33). A comparison of these values is given in Table III.

Determination of Arrhenius Activation Energies—The temperature dependence of the initial (30 s) velocity of enzyme preincubated with L-Phe corresponds to an activation energy for the catalytic process of 14.5 ± 1 kcal/mol subunit, compared to 12.0 kcal/mol subunit measured for the rat liver enzyme (33, 55). The use of stopped-flow detection methods for these activity measurements gave the same velocities as standard methods but more reproducible starting times.

The simulation of tyrosine buildup curves from standard (UV/visible spectra and stopped-flow) assay data afforded the simultaneous determination of both the catalytic (k_{cat}) and inactivation (k_{inact}) rates (Fig. 11). The temperature dependence of k_{cat} values from such simulations agreed well with simple linear approximation of tyrosine buildup in the first 30 s (UV/vis, 14.6 ± 0.6 kcal/mol subunit; stopped-flow, 14.6 ± 0.3 kcal/mol subunit). From simulated values of k_{inact}, we determined the kinetic barrier to irreversible inactivation to be 10 ± 1 kcal/mol subunit with a t½ of 4.3 min at 25, ° C.

The direct observation of the complex activation step (k_1 in Fig. 1) is more difficult with rPAH than with rat hepatic PAH

[4] It must be emphasized that there was no DTT present in this experiment to distinguish it from recent work that casts doubt on the copper requirement of a PAH from *Chromobacterium violaceum*. In that work, it is shown that a lag in catalysis is due to removal of inhibitory copper from the enzyme by DTT (85). Identical activities derive from assays of mammalian, iron-dependent enzyme in the presence or absence of DTT, which is often included to recycle oxidized pterin instead of NADPH/dihydropteridine reductase (31).

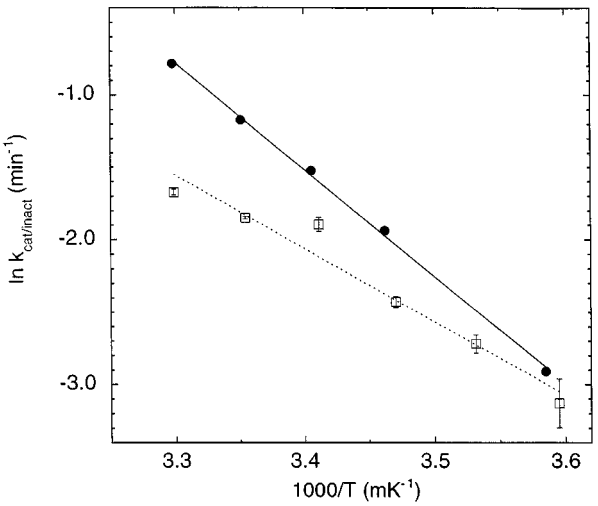

FIG. 11. **Arrhenius activation parameters under standard PAH assay conditions, analyzed by direct simulation using the model described in Fig. 1.** The temperature dependence of the initial velocity of reduced, L-Phe-preincubated enzyme corresponds to an activation energy for the catalytic process of 14.6 ± 0.6 kcal (mol subunit)$^{-1}$. An identical result was obtained from the stopped-flow assay method (14.6 ± 0.3 kcal mol^{-1}). The enzyme inactivates during L-Phe hydroxylation, with a half-life of 4.3 min at 25 °C. This process has an apparent activation energy of 10 ± 1 kcal (mol subunit)$^{-1}$. Standard assay data were obtained with 7 μg/ml rPAH (0.14 μM subunits) at a specific activity of 8 units/mg. The stopped-flow data that are shown in the figure were obtained with 5 μg/ml rPAH (0.1 μM subunits) at a specific activity of 6 units/mg. The *error bars* for the catalytic rate data fall within the symbols.

under identical assay conditions. Using a stopped-flow assay and 6-MPH$_4$ as cofactor, we were able to observe a significantly larger fraction of fully activated velocity present in the unpreincubated rPAH compared to authentic PAH. We were unable to find a value for k_1 by direct simulation with values of k_{cat} and k_{inact}, determined in parallel with L-Phe-preincubated enzyme, without resorting to the assumption that a fraction of unpreincubated rPAH is already in an R state (or determining a k_{cat} for rPAH^T). The reason for this discrepancy with PAH from different sources is unknown and is currently under investigation.

DISCUSSION

We report the overexpression in *E. coli* and characterization of recombinant PAH, which has kinetic and physical properties very similar to enzyme isolated from rat liver (Table III). The observation of tyrosine formation is only one of several important functional aspects of this enzyme. Other reports of PAH expression *in vitro* have appeared, but in neither of these has a complete description of these essential elements of PAH's mechanism been reported (22, 43). Such data will be required to understand individual mutations that cause PAH dysfunction and thereby PKU. It is not obvious from an examination of the nature or location of the PKU-associated mutations what is nonfunctional in PKU. Their distributed nature suggests that much of the highly conserved sequence of PAH is carefully balanced to achieve tight regulation of L-Phe catabolism and may be quite sensitive to even "conservative" amino acid substitutions. PAH's normal kinetic complexity reflects the requirement for several configurational changes in the enzyme, some of which may be disrupted or disfavored in PKU. The activities of several PKU mutants have been estimated, several with ~10% residual activity (21). While this can be physiologically quite serious, it may only be caused by a difference of a few kcal mol^{-1} in one of the activation barriers for allosteric activation, catalysis, or some other essential feature of PAH. To establish a solid linkage of phenotype with genotype, one needs a detailed structural description of PAH and PAH variants.

As isolated from rat liver, the specific activity of PAH varies from batch to batch in a manner that is attributable to the fraction of "active" iron, as distinguished from sites containing "inactive" iron. Inactive iron cannot perform the hydroxylation reaction, and efforts to restore it to an active state have proven unsuccessful (3). Inactivation of catalytically competent iron sites is particularly rapid during catalysis; the activity of PAH diminishes in a first-order manner (33) with a half-life of 4.3 min at 25 °C. In addition to the uneven phosphorylation of PAH, allelic heterogeneity is present in the common strains of laboratory rats (73). The fact that PAH forms a tetrameric structure amplifies all of these sources of heterogeneity. By heterologous expression of a single allele of rat hepatic PAH, we avoid a number of these problems. There are no known post-translational modifications of PAH (8, 46, 74) other than phosphorylation (which is easily performed by purified protein kinase (75, 76)), that would require expression of PAH in a eukaryotic cell line. In addition, *E. coli* does not contain a suitable pteridine cofactor (77), which prevents induced rPAH from performing hydroxylation, and thereby autoinactivating, prior to purification. This results in our observation that nearly all of the rPAH-associated iron is bound in the "active" configuration. The successful overexpression of this oligomeric, mammalian protein in *E. coli* is in conflict with assertions to the contrary (22) and in agreement with a similar accomplishment by Kaufman and co-workers (43).[5]

Overexpression of active rPAH tetramers in *E. coli* confirms that correct quaternary assembly occurs. When activated, rPAH can consume L-Phe at the same rate as rat liver PAH. The recombinant enzyme also shows inhibition of PAH activity at low levels of substrate; this sigmoidal response to L-Phe is indicative of allosteric behavior. *In vivo*, L-Phe levels may depend directly upon PAH allostery, since they are not depleted below a threshold value equal to the steepest part of PAH's *in vitro* activation response (33). Allosteric activation occurs in the rPAH protein following incubation with either L-Phe or lysolecithin, the most commonly used activators of the rat hepatic enzyme. Activation is correlated with characteristic structural changes in the rPAH enzyme as well as the expected increase in initial activity. Light scattering and gel filtration experiments performed on rPAH^T and rPAH^R indicate that there is a significant increase in the tetramer's size upon activation, which is consistent with the Monod, Wyman, and Changeux (MWC) model for an enzyme undergoing cooperative activation (78). The observed 3.6% increase in the solution radius is typical of allosteric proteins undergoing homotropic activation; *E. coli* aspartate transcarbamoylase undergoes a 5.4% increase upon binding of *N*-(phosphonacetyl)-L-aspartate (79), and yeast phosphofructokinase undergoes a 4.3% increase upon ATP binding (80). Lysolecithin activation at equilibrium has a small Hill coefficient, which is consistent with this structurally distinct compound activating PAH by a different mechanism than occurs during L-Phe activation. Regardless of the *mechanism* of activation, PAH$^R_{L\text{-Phe}}$ and PAH$^R_{lysolecithin}$ have essentially identical catalytic properties, including expanded substrate specificity, and are structurally similar, including a characteristic increase in hydrophobicity (3). In simply referring to "activation" or "activated enzyme," the mechanisms by which PAH becomes fully active are commingled with the kinetic characteristics of that state. We prefer the use of the Monod, Wyman, and Changeux nomenclature (T and R) to refer

[5] Other investigators have developed analogous systems for human PAH (86), TyrH (87–89), and TrpH (90, 91).

TABLE IV
Comparison of allosteric states of rPAH

	T state	R state
Oligomeric state	Tetramer	Tetramer
Stokes radius	55 Å[a] 51 ± 2 Å[b]	57 Å[a]
UV/visible spectra		
Native	λ_{max} = 278, 330 ε_M = 58000, 3000	λ_{max} = 278, 330 ε_M = 58000, 3000
Catechol adduct	λ_{max} = 698, 435 ε_M = 1900, ≈2000	λ_{max} = 698, 435 ε_M = 1900, ≈2000
Fluorescence emission		
λ_{max} (ex 293 nm)	333 nm	342 nm
k_q (KI, τ_o^{-1} M^{-1})[c]	0.92	1.4
k_q (acrylamide, τ_o^{-1} M^{-1})[c]	2.5	5.1
EPR		
(g_{eff}, Tris)	6.7, 5.4, 4.3	
(g_{eff}, MOPS)	Features from 600–1400 Gauss, 4.3	8.8, 4.5, 4.3
Fractional specific activity (units mg^{-1} Fe^{-1})	<0.9	10.5 ± 0.5

[a] From gel filtration.
[b] From dynamic light scattering.
[c] Stern-Volmer quenching coefficient at emission λ_{max}.

to the two particular configurations of PAH that are associated with distinct kinetic characteristics (78), distinguishing formal allosteric activation from generally stimulatory treatments. Some treatments that increase enzyme activity appear to arise from genuine changes in enzyme structure (high pH, phosphorylation, limited proteolysis), but others seem uncorrelated with such changes ("spontaneous activation" (4)).

A comparison of the spectroscopic properties of rPAH^T and rPAH^R is presented in Tables II and IV. While the observed differences in Stokes radii, fluorescence, and CD spectral data are consistent with an overall protein structural change upon conversion of rPAH^T to rPAH^R, the fate of the coordination environment about the iron center is less well defined. Although the energies of the LMCT bands in the optical spectra of native rPAH^T and rPAH^R as well as those of their respective catechol adducts are equivalent, suggesting that the iron primary coordination sphere remains relatively unchanged, the EPR spectra of these states clearly indicate a change in the iron site electronic structure. Owing to the similar affinities of the independent allosteric effector site (110 μM, pH 6.8) and the catalytic site (180 μM, pH 6.8) for L-Phe, it is expected that both sites will be fully occupied under the experimental conditions generally used for the complete conversion of rPAH^T to rPAH^R. We are therefore unable to fully assess whether the observed changes in the EPR spectra are a consequence of the effect of substrate in the active site or by changes in the iron coordination environment induced by the structural reorganization accompanying the rPAH^T to rPAH^R conversion. However, the electronic spectral data are consistent only with the former possibility. A more extensive study of the EPR and Mössbauer spectra of the various states available to rPAH will appear elsewhere.[6]

The absence of phosphate in the *E. coli*-expressed rPAH further confirms that the low, variable levels of phosphate content in liver protein are not required for, nor are they equivalent to, allosteric activation. The half-maximal activation response of unphosphorylated rPAH^T occurs at the same concentration as partially phosphorylated (0.2–0.3 phosphate per subunit) PAH. This suggests that the stimulatory effect of phosphorylation is not expressed at low levels of phosphate content. The observation of a K_{phe} identical to that of rat hepatic PAH confirms that phosphorylation affects only the regulatory L-Phe site; it does not perturb the active site L-Phe affinity or any catalytic properties. Only L-Phe and lysolecithin have been shown to cause a cooperative, sigmoidal activation response (at [effector] < 1 mM), using *either* BH_4 or 6-MPH_4. Phosphorylation sensitizes the enzyme to its substrate by lowering the concentration of L-Phe necessary for activation (9) without affecting the sigmoidal shape of the response, causing more effective *in vivo* catabolism (81).

Hydroxylation of L-Phe by rPAH requires molecular oxygen, L-Phe, and a pterin cofactor, with maximal activity at one atom of iron per subunit. The remarkable chemistry performed by PAH depends upon the correct positioning of these substrates near the active site iron. This occurs with either 6-MPH_4 or the natural cofactor BH_4. Variations in the structure or orientation of this side chain (or addition of a 7-substituent), which does not participate directly in the reaction, can lead to "uncoupling" of the hydroxylation of L-Phe from the oxidation of tetrahydropterin (82). Both pterins are efficiently used as cofactors for rPAH, but the initial time course of a standard assay using BH_4 has a pronounced curvature (data not shown) that makes the assignment of initial velocities difficult. Shiman and co-workers (11) have recently reported similar but less pronounced phenomena in a study of rat hepatic PAH, which they ascribed to BH_4-dependent relaxation of the activated enzyme (R → T) (11). The inhibitory characteristics of BH_4 are well known, among them prevention of substrate activation (3) and inhibition of phosphorylation (9). Full phosphorylation of the enzyme may obliterate the BH_4 regulatory site (9). The observations are consistent with BH_4 acting as a classic negative allosteric effector, *i.e.* one that preferentially binds to and stabilizes the T state. The determination of an Arrhenius activation energy for rPAH's allosteric activation has been hampered by a kinetic difference in the T → R conversion process of rPAH. However, activation by L-Phe *at equilibrium* causes 12-fold stimulation of the initial velocity, occurs at the same concentrations of applied activator, and yields a similar Hill coefficient.

Prereduction of ferric PAH is required for activity and can be detected as an initial absorbance decrease in a standard assay of oxidized rPAH^R performed on a stopped-flow. Reduced PAH^R binds both of its substrates and a molecule of O_2, which is activated for hydroxylation within a complex of pterin, L-Phe, and {Fe^{2+}} PAH. The mechanism of O_2 activation and the identity of the hydroxylating intermediate are unknown. Pterin does not appear to coordinate directly to the active iron (83) but is generally accepted to be an essential component of the active site. The catechol and NO adducts of the ferric and ferrous forms of the enzyme will be quite useful in assessing the catalytic importance of vacant iron coordination sites, in the presence and absence of the tetrahydropterin coenzyme.

Earlier studies designed to examine the steady state equilibrium kinetic mechanism of PAH were apparently performed prior to the realization that thorough preactivation of PAH is required for maximal enzyme activity. The determination of a sequential mechanism for PAH indicates that all three substrates are ordered at the active site before any product is released. Reliance upon L-Phe activation under steady state conditions severely limits the range of concentrations available for study (72). The L-Phe activated results alone do not allow the assignment of a sequential or ping-pong mechanism since parallel and intersecting lines are difficult to distinguish over a narrow range of substrate concentrations (84). Lysolecithin allows the assay of rPAH at low concentrations of [L-Phe] without complications due to the activator role of this substrate. Lysolecithin was maintained at ≥0.5 mM throughout the modified standard assay to ensure stable activation of rPAH. In this way, the double-reciprocal analysis of PAH at

[6] E. Glasfeld, Y. M. Xia, P. G. Debrunner, and J. P. Caradonna, manuscript in preparation.

saturating O_2 has been extended across more than 3 orders of magnitude of [L-Phe] centered upon its K_{app}. This study confirms that a sequential mechanism is operative in rPAH under conditions of lysolecithin activation, where the L-Phe-activated results are ambiguous at best. At high levels of L-Phe and at $[6\text{-MPH}_4] \leq 0.5\ K_{m,6\text{-MPH}_4}$, the slightly lower velocities typical of substrate inhibition were observed. This effect, although much less pronounced, was also observed in double-reciprocal analysis of L-Phe-activated enzyme. Concentrations of $[6\text{-MPH}_4]$ high enough to observe pterin inhibition were not encountered during either experiment, as both of these studies were limited by the background autooxidation of $[6\text{-MPH}_4]$ to low levels of this cofactor ($\leq 3\ K_{app}$). Significant substrate inhibition with lysolecithin-activated rPAH (at any $[6\text{-MPH}_4]$) below 2 mM L-Phe was not observed, in contrast with a previous report that such inhibition begins above 0.3 mM L-Phe (13).

In summary, we have compared the kinetic requirements of rPAH to rat hepatic PAH in detail and find that the recombinant enzyme recapitulates every catalytic detail. There is stimulation of the rate of hydroxylation following exposure to the same allosteric activators; rPAH has the same requirement for reduced iron and the same affinity for its substrates. The temperature dependence of the catalytic step of rPAH yields a similar kinetic activation energy barrier. In addition, we have measured an Arrhenius activation barrier for the poorly understood kinetic inactivation process of PAH. Overexpressed rPAH is synthesized quickly (in 6 h *versus* several days for a eukaryotic expression system (22)) in an environment free of pterin cofactor and general phosphorylating conditions, which results in a homogeneous preparation free of complications due to inactive iron and uneven phosphorylation. By many structural criteria, rPAH is essentially equivalent to rat hepatic PAH.

The availability of this source of rPAH will aid in the resolution of several long-standing issues pertaining to the chemistry and structure of PAH. One of the most important is the nature of the allosteric activation process (T → R conversion), which we have shown by UV-visible spectra and CD spectroscopy causes only minor changes in the carboxylate/histidine coordination environment of the active site iron and the overall secondary structure of the protein. There is at least one partially accessible, labile coordination site on the iron (Fe^{3+} and Fe^{2+}) present in T state rPAH, demonstrated by the ready formation of Tris, catechol, and NO adducts. However, $rPAH^T$ is able to preclude access to the iron site by its substrates, directing them instead to the allosteric L-Phe site and the pterin reduction site, which are functionally and/or spatially distinct from the $rPAH^R$ active site. In support of this, EPR spectra show that both T and R state PAH have mostly rhombic active site environments, but in the latter case increased L-Phe accessibility to the active site causes perturbations due to its binding near the iron.[6] Spectroscopic data are consistent with the immediate iron environment being relatively insensitive to the allosteric state of the enzyme. Characteristic fluorescence shifts, increased hydrophobicity, a large activation energy barrier, and a 10% volume increase are suggestive of a large reconfiguration of the distant protein matrix following allosteric activation. This process can now be more reliably envisioned as resulting from the removal of an inhibitory portion of the protein, exposing a functional active site, rather than as a L-Phe-dependent rearrangement of the iron ligands.

Acknowledgments—We thank Profs. Donald Crothers (Yale University), Robert O. Fox (Yale and HHMI), and Steven Burley (Rockefeller University and HHMI) for the use of equipment. We thank Dr. Elizabeth Glasfeld for productive discussions and Dr. Michael Cascio for assistance with the CD data collection and analysis.

REFERENCES

1. Scriver, C. R., Eisensmith, R. C., Woo, S. L. C., and Kaufman, S. (1994) *Annu. Rev. Genet.* **28,** 141–165
2. Gottschall, D. W., Dietrich, R. F., Benkovic, S. J., and Shiman, R. (1982) *J. Biol. Chem.* **257,** 845–849
3. Shiman, R. (1985) in *Chemistry and Biochemistry of Pterins* (Blakely, R. L., and Benkovic, S. J., eds) pp. 179–249, John Wiley & Sons, Inc., New York
4. Kaufman, S. (1993) *Adv. Enzymol. Rel. Areas Mol. Biol.* **67,** 77–264
5. Kaufman, S. (1985) in *Chemistry and Biochemistry of Pterins* (Blakely, R. L., and Benkovic, S. J., eds) pp. 251–351, John Wiley & Sons, Inc., New York
6. Kuhn, D. M., and Lovenberg, W. (1985) in *Chemistry and Biochemistry of Pterins* (Blakely, R. L., and Benkovic, S. J., eds) pp. 353–382, John Wiley & Sons, Inc., New York
7. Marota, J. J., and Shiman, R. (1984) *Biochemistry* **23,** 1303–1311
8. Shiman, R. (1980) *J. Biol. Chem.* **255,** 10029–10032
9. Døskeland, A. P., Døskeland, S. O., Øgreid, D., and Flatmark, T. (1984) *J. Biol. Chem.* **259,** 11242–11248
10. Døskeland, A. P., Haavik, J., Flatmark, T., and Døskeland, S. O. (1987) *Biochem. J.* **242,** 867–874
11. Xia, T., Gray, D. W., and Shiman, R. (1994) *J. Biol. Chem.* **269,** 24657–24665
12. Kaufman, S. (1987) in *The Enzymes* (Boyer, P. D., and Krebs, E. G., eds), 3rd Ed., pp. 217–282, Academic Press, Orlando, FL
13. Fisher, D. B., and Kaufman, S. (1973) *J. Biol. Chem.* **248,** 4345–4353
14. Renson, J., Goodwin, F., Weissbach, H., and Udenfriend, S. (1961) *Biochem. Biophys. Res. Commun.* **6,** 20–23
15. Kaufman, S., and Mason, K. (1982) *J. Biol. Chem.* **257,** 14667–14678
16. Miller, R. J., and Benkovic, S. J. (1988) *Biochemistry* **27,** 3658–3663
17. Siegmund, H. U., and Kaufman, S. (1991) *J. Biol. Chem.* **266,** 2903–2910
18. Lidksy, A. S., Robson, K. J., Thirumalachary, C., Barker, P. E., Ruddle, F. H., and Woo, S. L. C. (1984) *Am. J. Hum. Genet.* **36,** 527–533
19. Kay, M. A., and Woo, S. L. C. (1994) *Trends Genet.* **10,** 253–257
20. Knappskog, M., Eiken, H. G., Martínez, A., Olafsdottir, S., Haavik, J., Flatmark, T., and Apold, J. (1993) *Adv. Exp. Med. Biol.* **338,** 59–62
21. Okano, Y., Eisensmith, R. C., Guttler, F., Lichter-Konecki, U., Konecki, D. S., Trefz, F. K., Dasovich, M., Wang, T., Henriksen, K., Lou, H., and Woo, S. L. C. (1991) *New Engl. J. Med.* **324,** 1232–1238
22. Gibbs, B. S., Wojchowski, D., and Benkovic, S. J. (1993) *J. Biol. Chem.* **268,** 8046–8052
23. Dahl, H.-H. M., and Mercer, J. F. B. (1986) *J. Biol. Chem.* **261,** 4148–4153
24. Tipper, J., and Kaufman, S. (1992) *J. Biol. Chem.* **267,** 889–896
25. Shiman, R., Akino, M., and Kaufman, S. (1971) *J. Biol. Chem.* **246,** 1330–1340
26. Storm, C. B., Shiman, R., and Kaufman, S. (1971) *J. Org. Chem.* **36,** 3925–3927
27. Studier, F. W., and Moffatt, B. A. (1986) *J. Mol. Biol.* **189,** 113–130
28. Maniatis, T., Fritsch, E. F., and Sambrook, J. (1982) *Molecular Cloning: A Laboratory Manual*, Cold Spring Harbor Laboratory Press, Cold Spring Harbor, NY
29. Studier, F. W., Rosenberg, A. H., Dunn, J. J., and Dubendorff, J. W. (1990) *Methods Enzymol.* **185,** 60–89
30. Hanahan, D. (1983) *J. Mol. Biol.* **166,** 557–580
31. Shiman, R. (1987) *Methods Enzymol.* **142,** 17–27
32. Shiman, R., Gray, D. W., and Pater, A. (1979) *J. Biol. Chem.* **254,** 11300–11306
33. Shiman, R., and Gray, D. W. (1980) *J. Biol. Chem.* **255,** 4793–4800
34. Wallick, D. E., Bloom, L. M., Gaffney, B. J., and Benkovic, S. J. (1984) *Biochemistry* **23,** 1295–1302
35. Beck, W. F., Innes, J. B., and Brudvig, G. W. (1991) *J. Magn. Reson.* **91,** 12–29
36. Yonetani, T., Yamamoto, H., Erman, J. E., Leigh, J. S., Jr., and Reed, G. H. (1972) *J. Biol. Chem.* **247,** 2447–2455
37. Arciero, D. M., Orville, A. M., and Lipscomb, J. D. (1985) *J. Biol. Chem.* **260,** 14035–14044
38. Siegel, L. M., and Monty, K. J. (1966) *Biochim. Biophys. Acta* **112,** 346–362
39. Wilkinson, G. N. (1961) *Biochem. J.* **80,** 324–337
40. Barshop, B. A., Wrenn, R. F., and Frieden, C. (1983) *Anal. Biochem.* **130,** 134–145
41. Zimmerle, C. T., and Frieden, C. (1989) *Biochem. J.* **258,** 381–387
42. Shiman, R., and Jefferson, L. S. (1982) *J. Biol. Chem.* **257,** 839–844
43. Citron, B. A., Davis, M. D., and Kaufman, S. (1992) *Protein Expression Purif.* **3,** 93–100
44. Zimmerman, J. K., and Ackers, G. K. (1971) *J. Biol. Chem.* **246,** 7289–7292
45. Traut, T. W. (1994) *Crit. Rev. Biochem. Mol. Biol.* **29,** 125–163
46. Nakata, H., and Fujisawa, H. (1980) *Biochim. Biophys. Acta* **614,** 313–327
47. Pistorius, E. K., Axelrod, B., and Palmer, G. (1976) *J. Biol. Chem.* **251,** 7144–7148
48. Egmond, M. R., Finazzi-Agro, A., Fasella, P. M., Veldink, G. A., and Vliegenthart, J. F. (1975) *Biochim. Biophys. Acta* **397,** 43–49
49. Slykhouse, T. O., and Fee, J. A. (1976) *J. Biol. Chem.* **251,** 5472–5477
50. Yost, F. J., Jr., and Fridovich, I. (1973) *J. Biol. Chem.* **248,** 4905–4908
51. Asada, K., Yoshikawa, K., Takahashi, M., Maeda, Y., and Enmanji, K. (1975) *J. Biol. Chem.* **250,** 2801–2807
52. Phillips, R. S., Parniak, M. A., and Kaufman, S. (1984) *Biochemistry* **23,** 3836–3842
53. Shiman, R., Jones, S. H., and Gray, D. W. (1990) *J. Biol. Chem.* **265,** 11633–11642
54. Chang, C. T., Wu, C.-S. C., and Yang, J. T. (1978) *Anal. Biochem.* **91,** 12–31
55. Abita, J. P., Parniak, M., and Kaufman, S. (1984) *J. Biol. Chem.* **259,** 14560–14566
56. Cox, D. D., Benkovic, S. J., Bloom, L. M., Bradley, F. C., Nelson, M. J., Que, L. J., and Wallick, D. E. (1988) *J. Am. Chem. Soc.* **110,** 2026–2032
57. Bradley, F. C., Lindstedt, S., Lipscomb, J. D., Que, L., Jr., Roe, A. L., and Rundgren, M. (1986) *J. Biol. Chem.* **261,** 11693–11696
58. Whittaker, J. W., Lipscomb, J. D., Kent, T. A., and Münck, E. (1984) *J. Biol. Chem.* **259,** 4466–4475
59. Yang, A.-S., and Gaffney, B. J. (1987) *Biophys. J.* **51,** 55–67
60. Gaffney, B. J., Mavrophilipos, D. V., and Doctor, K. S. (1993) *Biophys. J.* **64,**

773–783
61. Bloom, L. M., Benkovic, S. J., and Gaffney, B. J. (1986) *Biochemistry* **25,** 4204–4210
62. Andersson, K. K., Cox, D. D., Que, L., Jr., Flatmark, T., and Haavik, J. (1988) *J. Biol. Chem.* **263,** 18621–18626
63. Andersson, K. K., Haavik, J., Martinez, A., Flatmark, T., and Petersson, L. (1989) *FEBS Lett.* **258,** 9–12
64. Solomon, E. I., and Zhang, Y. (1992) *Acc. Chem. Res.* **25,** 343–352
65. Enemark, J. H., and Feltham, R. D. (1974) *Coord. Chem. Rev.* **13,** 339–406
66. Brown, C. A., Pavlosky, M. A., Westre, T. E., Zhang, Y., Hedman, B., Hodgson, K. O., and Solomon, E. I. (1995) *J. Am. Chem. Soc.* **117,** 715–732
67. Chen, V. J., Orville, A. M., Harpel, M. R., Frolik, C. A., Surerus, K. K., Münck, E., and Lipscomb, J. D. (1989) *J. Biol. Chem.* **264,** 21677–21681
68. Deligiannakis, Y., Tsekos, N., Petrouleas, V., and Diner, B. A. (1992) *Biochim. Biophys. Acta* **1140,** 163–168
69. Arciero, D. M., Lipscomb, J. D., Huynh, B. H., Kent, T. A., and Münck, E. (1983) *J. Biol. Chem.* **258,** 14981–14991
70. Salerno, J. C., and Siedow, J. N. (1979) *Biochim. Biophys. Acta* **579,** 246–251
71. Rich, P. R., Salerno, J. C., Leigh, J. S., and Bonner, W. D. (1978) *FEBS Lett.* **93,** 323–326
72. Kaufman, S., and Fisher, D. B. (1974) in *Molecular Mechanisms of Oxygen Activation* (Hayaishi, O., ed) pp. 285–369, Academic Press, New York
73. Mercer, J. F., McAdam, W., Chambers, G. W., and Walker, I. D. (1986) *Biochem. J.* **236,** 679–683
74. Døskeland, A., Ljones, T., Skotland, T., and Flatmark, T. (1982) *Neurochem. Res.* **7,** 407–421
75. Abita, J. P., Milstien, S., Chang, N., and Kaufman, S. (1976) *J. Biol. Chem.* **251,** 5310–5314
76. Milstien, S., Abita, J. P., Chang, N., and Kaufman, S. (1976) *Proc. Natl. Acad. Sci. U. S. A.* **73,** 1591–1593
77. Sawada, M., and Nagatsu, T. (1987) in *Unconjugated Pterins in Neurobiology* (Lovenberg, W., and Levine, R. A., eds) Vol. 1, pp. 131–156, Taylor & Francis, Philadelphia
78. Monod, J., Wyman, J., and Changeux, J.-P. (1965) *J. Mol. Biol.* **12,** 88–118
79. Moody, M. F., Vachette, P., and Foote, A. M. (1979) *J. Mol. Biol.* **133,** 517–532
80. Laurent, M., Tijane, M. N., Roucous, C., Seydoux, F. J., and Tardieu, A. (1984) *J. Biol. Chem.* **259,** 3124–3126
81. Shiman, R., Mortimore, G. E., Schworer, C. M., and Gray, D. W. (1982) *J. Biol. Chem.* **257,** 11213–11216
82. Storm, C. B., and Kaufman, S. (1968) *Biochem. Biophys. Res. Commun.* **32,** 788–793
83. Shiman, R., Xia, T., Hill, M. A., and Gray, D. W. (1994) *J. Biol. Chem.* **269,** 24647–24656
84. Bar-Tana, J., and Cleland, W. W. (1974) *J. Biol. Chem.* **249,** 1263–1270
85. Carr, R. T., and Benkovic, S. J. (1993) *Biochemistry* **32,** 14132–14138
86. Martínez, A., Knappskog, P. M., Olafsdottir, S., Døskeland, A. P., Eiken, H. G., Svebak, R. M., Bozzini, M., Apold, J., and Flatmark, T. (1995) *Biochem. J.* **306,** 589–597
87. Daubner, S. C., Lauriano, C., Haycock, J. W., and Fitzpatrick, P. F. (1992) *J. Biol. Chem.* **267,** 12639–12646
88. Haavik, J., Le Bourdelles, B., Martínez, A., Flatmark, T., and Mallet, J. (1991) *Eur. J. Biochem.* **199,** 371–378
89. Wang, Y. H., Citron, B. A., Ribeiro, P., and Kaufman, S. (1991) *Proc. Natl. Acad. Sci. U. S. A.* **88,** 8779–8783
90. Yang, X. J., and Kaufman, S. (1994) *Proc. Natl. Acad. Sci. U. S. A.* **91,** 6659–6663
91. Park, D. H., Stone, D. M., Kim, K. S., and Joh, T. H. (1994) *Mol. Cell. Neurosci.* **5,** 87–93
92. Kaufman, S. (1987) *Methods Enzymol.* **142,** 3–17
93. Petrouleas, V., and Diner, B. (1990) *Biochim. Biophys. Acta* **1015,** 131–140
94. Glasfeld, E. (1994) *The Spectroscopic Characterization of the Non-Heme Iron Active Site of Phenylalanine Hydroxylase*, Ph.D. thesis, Yale University
95. Nielsen, K. H. (1969) *Eur. J. Biochem.* **7,** 360–369